coatings

MDPI

Article

Milling of Complex Surfaces of EN 10060 Steel after HVOF Sprayed NiCrBSi Coatings

Jan Valíček [1], Marta Harničárová [1,*], Jan Řehoř [1], Milena Kušnerová [1], Jaroslava Fulemová [1], Miroslav Gombár [1], Ludmila Kučerová [1], Jan Filipenský [2] and Jan Hnátík [1]

[1] Regional Technology Institute, Faculty of Mechanical Engineering, University of West Bohemia, Univerzitni 8, 306 14 Pilsen, Czech Republic; valicekj@rti.zcu.cz (J.V.); rehor4@kto.zcu.cz (J.Ř.); milena.kusnerova@gmail.com (M.K.); fulemova@kto.zcu.cz (J.F.); gombar@kto.zcu.cz (M.G.); skal@rti.zcu.cz (L.K.); jhnatik@kto.zcu.cz (J.H.)

[2] PLASMAMETAL, spol. s r. o., Tovární 917/1e, 643 00 Brno-Chrlice, Czech Republic; filipensky@plasmametal.cz

* Correspondence: marta.harnicarova@gmail.com or marta.harnicarova@uniag.sk

Received: 30 June 2020; Accepted: 28 July 2020; Published: 30 July 2020

Abstract: The high-velocity oxy-fuel spraying process was used to investigate and improve the surface properties of a workpiece. The research was focused on the spherical surface of a workpiece made of high-strength steel, a ball and socket assembly. After spraying with a nickel alloy, the surface was machined by milling. The coating was carried out as a process in which a very thin layer of coating of the required thickness and the required specific properties, i.e., high Vickers hardness, adhesion to the surface, wear resistance and other important characteristics, which must be respected in other machining methods, was applied to the already finished, heat-prepared metal substrate. This article deals with the milling of complex surfaces of steel substrate EN 10060 after spraying with NiCrBSi alloy. After spraying, a total of 15 milling experiments were performed in order to determine precisely the optimal cutting parameters of milling and surface adhesion, based on newly acquired prediction relations. The main presented results are new relations for the determination of optimal technological milling conditions based on the identification of adhesive sections using derived equations. The new relations were verified and also compared with the current literature in the field.

Keywords: spraying; coating; milling; surface roughness; surface Vickers hardness

1. Introduction

The aim of the application of coatings created by high-velocity oxy-fuel is the modification or restoration of functional surfaces with specific properties on machine parts while reducing production and operating costs [1–3]. This technology remains of interest for many researchers, although it is 40 years old. It is possible to use this technology in the field of primary production, as well as in the field of repairs and renovations. During the coating process, the base material is heated to a temperature close to 100 °C, in exceptional cases, up to 150 °C. Thus, there is neither deformation of the coated part nor degradation of the structure of the base material. The first published work on warm spraying was found in 2006 [4]. In general, the thermal spray coating process can be characterized as the melting of additive material (in the form of a powder, wire, or rod), the particles of which are accelerated and applied to a preprepared, degreased, and blasted surface of the base material [5]. Upon impact with the substrate, the individually incident particles are partially or entirely deformed; they cool down very rapidly, solidify, and form a typical heterogeneous coating structure, which is gradually

homogenized. Commonly available coating thicknesses range from 0.1 mm to several millimetres, depending on the technology used.

Coatings created by thermal spraying technology can be applied to all common construction materials (ferrous and nonferrous metals). Thus, when applying materials using the thermal spraying technology, neither the chemical composition of the basic material of the repaired part or the part whose protection we are monitoring, nor its condition are significant.

During the process of coating using the thermal spraying technology [6], the base material is not heated above 100 °C, in exceptional cases, it is heated to 150 °C, i.e., during the application of the coating material, there is neither deformation of the coated part nor degradation of the structure due to thermal effects on the base material.

Always should be taken into account the selection of coatings according to the specific needs and conditions of use. Most corrosion- and heat-resistant alloys rely on the formation of an oxide film to provide corrosion resistance. Chromium oxide is the most common of such films. NiCrBSi coatings have been developed for applications requiring excellent wear and corrosion resistance with service temperatures up to 850 °C. Nowadays, high-temperature corrosion is a severe problem in the field of energy equipment design. Several different measures are used in the "fight" against high-temperature corrosion. However, it can be stated that most of them either prevent high-temperature corrosion or reduce it only partially and temporarily. The application of protective coatings created by HVOF technology, therefore, appears to be one of the most effective options for protecting components against such attack.

Many research studies have been done to examine NiCrBSi coatings produced by the HVOF technique. Most of them are focused on the study of NiCrBSi microstructure, Vickers hardness, friction, and wear performance. Planche et al. [7] made a comparison of NiCrBSi coatings made by different thermal spraying processes (plasma, flame, HVOF). Properties such as hardness, porosity or Young modulus were found better for the HVOF coatings and were strongly dependent on the in-flight velocities of the particles. A similar study was made by Modi at al [8]. The XRD analysis showed differences in the phase composition when using HVOF and spray and fuse technology. The explanation of the role of plastic deformation during wear has been explained by Garrido et al. [9]. Description of phase transformation NiCrBSi–WC coatings prepared by electric arc spray can be found in [10]. Zouari et al. [11], Miguel et al. [12] and Gonzalez [13] described the differences in tribological properties of NiCrBSi coatings prepared by different technologies.

An interesting comparison was made by Houdková et al. [14]. They studied the mechanical properties, microstructure, wear and friction properties of thermally sprayed NiCrBSi coatings with consequent post-heat-treatment by different technologies. The process of remelting had a positive effect on wear and corrosion resistance due to the improvement of coating adhesion. However, it was observed that there was little effect on sliding wear (independent of used remelting technology). Chaliampalias et al. [15] studied the microstructure and morphology of NiCrBSi coatings prepared by flame spraying technology. Low carbon steel was used as a substrate. Except for the presence of Ni and Ni–Cr phases, it was also observed a layer of Cr_2O_3 in the thickness of a few nanometers. There is another interesting study [16] of the NiCrBSi coatings with a different extent of tungsten carbide particles prepared by the flame method on spring steel. By adding WC into the coating, the wear resistance, and the hardness of NiCrBSi matrix were increased.

Mechanical special parts and components like gears, or rolling bearings are subjected to high wear due to surface damage generated by rolling contact, which affects the life of the components. Therefore, it is essential to investigate the effect of coatings on the substrate and to find out what type of coatings should be used for certain applications and under different conditions. Practical solutions for coatings are found [17].

Coatings are used to have friction and wear under control in all kinds of contacts. In many industrial processes, for special applications, spherical surface parts are often used. For these parts, advanced knowledge of coating technology is necessary because the process of obtaining excellent

results in coatings is more complicated than on a flat surfaces. The substrate/coating interface at the spherical contact during loading was studied by several authors. Zhang et al. [18] were trying to develop the coating thickness prediction for a spherical contact. Their model can be used in practice for the robotic thermal spray system to predict the coating thickness on nonholonomic spherical surfaces.

The coated spherical contact was of interest also for other researchers [19,20]. There are some models being developed, which allow a thorough understanding of the spherical coated surface under different loading modes. The research teams of [21,22] also discussed the problems of coating thickness evolution and uniformity on a spherical surface in the case of integrated circuit manufacturing.

A real coating cannot be perfectly homogeneous or compact because the very nature of the formation of the coating creates the conditions for the formation of pores, or other accompanying phenomena (such as oxides), occurring during the thermal spraying of some metallic materials (iron-based) in a standard atmosphere. The state-of-the-art coating method—high-speed continuous detonation deposition—makes it possible to create coatings whose structure can be assessed as relatively homogeneous, with high values of cohesion and adhesion to the substrate and with low porosity values (below 1%) [23,24]. It means that due to the applied method of thermal spraying technology, technological parameters, the type and form of material used, the structure of the applied coating and thus also the basic properties of the coating differ significantly. The following parameters can be included among the basic properties of coatings: adhesion of the coating to the base material (adhesion), the cohesion of the coating (cohesion), the porosity of the coating, Vickers hardness, fracture toughness, thermal expansion, electrical properties.

When verifying the above properties, it is decisive whether the tests are performed on testing machines, possibly directly under operating conditions, or on experimental equipment that only simulates the operating conditions and effects on the coating. With these experimental devices, it is complicated to simulate the specific working conditions in a given device, so the results obtained when comparing different types of materials can be misleading in some cases.

Hot spraying generates a characteristic structure of the coating material that differs significantly from homogeneous materials. The quality of the homogenization of the transition from the substrate to the coating from a mechanical point of view mainly depends on the topographic parameters of the substrate surface. Based on experimental knowledge, new methods of exact selection of a combination of cutting parameters for controlling the desired surface condition of both the substrate and the spraying are proposed in the presented work. The intensity of the adhesive stress and adhesive forces is determined by the quality of the homogenization of the transition between the substrate and the coating.

Based on literature research, we can conclude that there is a limited number of published papers dealing with the determination of the machining parameters of NiCrBSi coatings sprayed on surfaces with complex geometries. The presented publication was created in order to improve the surface properties of a spherical steel surface after HVOF spraying of a nickel alloy, which is subsequently machined by milling.

2. Materials and Methods

2.1. Base Material—Steel EN 10060

Steel EN 10060 (34CrNiMo6) was chosen as the base material, which is used for highly stressed machine parts with an emphasis on the required toughness, strength, and Vickers hardness of the material. This material was purchased to make the ball and socket assembly. Table 1 shows the chemical composition of the base material used at 23 °C.

Table 2 lists the key parameters of the sample from the base material used according to the tensile diagram made after the standardized tensile test, namely yield strength, contraction, ductility as quantified plastic deformability before reaching the yield strength, and material yield strength.

Table 1. Chemical composition.

Chemical Composition	C	Si	Mn	P	Cr	Mo	Ni	Cu	Sn
wt.%	0.34	0.36	0.58	0.01	1.62	0.29	1.63	0.06	0.005

Table 2. Tensile test performed at 23 °C.

Parameters	R_m [1] MPa	$R_{p0.2}$ [1] MPa	A_5 [1] GPa	Z [1] %
EN 10060	1024	932	17.3	62

[1] R_m—material strength, $R_{p0.2}$—yield strength, A_5—ductility, Z—contraction.

2.2. Spray Material—NiCrBSi Alloy

The coating of the examined sample was applied to the prepared substrate, according to the required experimental conditions:

- additional material: NiCrBSi, Vickers hardness 58–60 HRC, grain size 20–53 µm;
- machining of the generated surface by milling.

Figure 1 presents the morphological results of NiCrBSi powder spraying obtained by scanning electron microscopy (SEM, Semilab Germany GmbH, Braunschweig, Germany) (Figure 1a,b) and analysis of this spraying by Energy dispersive X-Ray (EDX) technique (Bruker, Ewing, NJ, USA), commonly used in electron microscopy (Figure 1c,d).

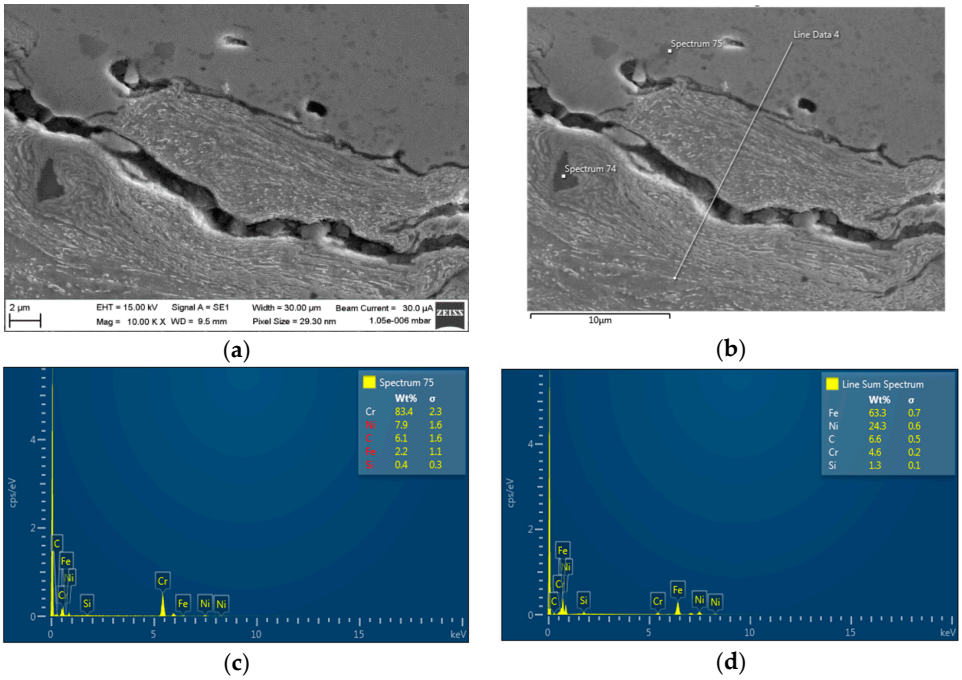

(**a**) (**b**)

(**c**) (**d**)

Figure 1. Morphology of NiCrBSi powder: (**a**,**b**) NiCrBSi powder spraying obtained by scanning electron microscopy; (**c**,**d**) EDX analysis of NiCrBSi powder.

2.3. Milling the Surface of the Base Material after Spraying

The experiment is based on the results of direct measurements of three basic cutting parameters (Table 3), namely: speed of cut v_c (m·min^{-1}), feed per tooth f_z (mm), and the depth of cut a_p (mm). The machining parameters mentioned above can be considered as technologically basic because they express the machined volume of material, the structure and texture of the machined surface, as well as its instantaneous stress-strain state. In addition to the final surface topography, they describe the

stress-strain volume of the affected material at the contact of the cutting knife with the disintegrated material. The quality of homogenization of this transition determines the intensity of the adhesive stress and the action of the adhesive forces. The milling of the surface of the EN 10060 material after NiCrBSi spraying was performed on a linear milling centre DMU 40 eV olinear (DMU 40 eV olinear (DMG MORI, Pfronten, Bavaria, Germany). It is a new generation DMU eVo machine with a perfect interaction of the performance potential of the universal milling cutter and the vertical machining centre.

Table 3. Basic cutting parameters: the speed of cut v_c, the feed per tooth f_z, the depth of cut a_p.

E_{xpNo}	v_c (m·min^{-1})	f_z (mm)	a_p (mm)
1	700	0.15	0.15
2	450	0.15	0.15
3	500	0.15	0.15
4	400	0.15	0.15
5	500	0.2	0.20
6	500	0.1	0.10
7	500	0.25	0.25
8	500	0.3	0.30
9	500	0.2	0.25
10	500	0.2	0.30
11	500	0.25	0.20
12	500	0.25	0.30
13	500	0.3	0.20
14	500	0.3	0.25
15	500	0.25	0.25

In order to examine the influence of the choice of cutting parameters, it can be stated that the combinations of selected parameters were selected arbitrarily and, to a large extent, subjectively, because even in current technical practice, there are still no relations of targeted, exactly continuous choice. The individual combinations of cutting parameters are listed in Table 3 under Section 2.3.

For the required depth of cut, workpiece width, tool diameter and the number of teeth, the recommended cutting conditions can be found commonly in machine tables, but only for machining relatively simple surfaces, most often planar. For complex surfaces, which spherical surfaces undoubtedly are, such optimization guidelines do not yet exist. Therefore, we applied an empirical approach when milling a specific coating, i.e., so that the machining of difficult-to-machine surfaces is feasible.

The experimental part of the paper is focused on investigating the influence of specifically defined combinations of cutting parameters in the machining of selected materials (NiCrBSi alloy and EN 100 60 metal). In the experiments, a total of 15 cuts were made by milling on a sprayed coating layer of NiCrBSi alloy.

The primary goal for milling the studied coating is to generate a homogeneous coating of constant thickness, with the desired adhesiveness, Vickers hardness, and surface roughness. However, the production process is not only about setting the optimal technological parameters (speed of cut, feed per tooth and depth of cut), but also about the efficient use of the cutting insert. The cutting insert edge must be changed because it heats up and wears out during milling. For this reason, 15 experiments on 15 spherical workpiece surfaces were divided into three groups, each consisting of 5 experiments, with just one cutting edge being used in one experiment.

For a group of experiments 1–5 of A section, optimal technological parameters were searched. At higher speeds of cut (above 500 m·min^{-1}), the cutting edge even jammed, at lower speeds of cut (below 500 m·min^{-1}) the surface was machined unevenly to a significant degree, so there were relatively deep irregularly spaced holes or larger hollows.

For a group of experiments 6–15, the optimally found speed of cut of 500 m·min^{-1} was used, and the remaining values of technological parameters were combined so that the feed per tooth and the depth of cut were measured in an empirically verified interval of 0.1 to 0.3 mm with a step of 0.05 mm. The relative machinability parameter R_{mp} showed an information value for the comparison of the results in terms of the necessary roughness and adhesive stress of the generated coatings. According to this newly introduced decision criterion, experiments 6–10 of B section were classified as the section with satisfactory surface roughness for the desired adhesion, and experiments 11–15 of C section were classified as the section with excellent surface roughness for the desired adhesion.

2.4. Measurement of Roughness and Vickers Hardness

The microtexture of the machined area was measured with an ALICONA non-contact-optical profilometer (Alicona Imaging GmbH, Raaba, Austria). A lens with 50× magnification was used to scan the planar and surface roughness of the surface.

The Vickers hardness of the machined area was measured after imprints using a Vickers hardness tester (M-400-A, LECO, St. Joseph, MI, USA), at a selected value of a loading force of 300 gf. The Vickers hardness value was calculated using the measured lengths of the imprint diagonals (the boundary lines located in the ocular were set to be located at the opposite corners of the imprint). The maximum accuracy of length measurement was 7 µm; specifically, in the case of steel 5 to 6 µm, in the case of NiCrBSi coating about 4 µm. Because the Vickers hardness varies depending on the cutting directions due to the characteristic anisotropy of the microstructure of thermal sprays, the Vickers hardness of the substrate and the spraying were measured on metallographic cuts perpendicular to the surface of the coatings.

The average Vickers hardness was calculated [25,26] for each sample according to Equation (1):

$$HV = \frac{2 \cdot F \cdot \sin\left(\frac{\alpha}{2}\right)}{g \cdot d^2} \approx 0.189 \cdot \frac{F}{d^2} \quad (1)$$

where HV is the Vickers hardness, F is the applied force (N), α is the mean angle between the opposite faces at the vertex of the pyramidal indenter (for the nominal angle α = 136°), d is the arithmetic mean of the two diagonal lengths d_1 and d_2 (mm), and g is the gravitational acceleration (m·s^{-2}) 9.807.

The distribution functions of selected cutting parameters for the calculation of the parameters R_{mp} and R_{mp0} were related to the depth of cut a_p.

Figure 2 describes the dependence of the Vickers hardness of the substrate and the coating on the depth of cut, according to the approximation relations (2) and (3).

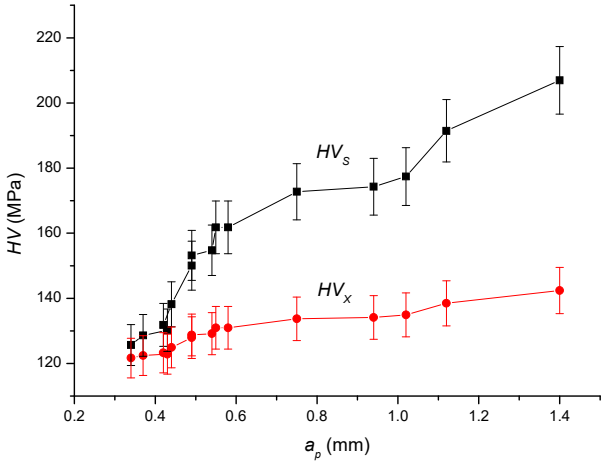

Figure 2. Dependence of Vickers hardness on the depth of cut (HV_S—substrate Vickers hardness; HV_X—spray Vickers hardness).

Equation (2) applies to substrate Vickers hardness and Equation (3) applies to spray Vickers hardness at a depth of cut with an accuracy of $R^2 = 0.93$:

$$HV_S = 83.77 + 148.56 \cdot a_p - 46.13 \cdot a_p^2 \quad (2)$$

$$HV_X = 110.92 + 38.25 \cdot a_p - 12.00 \cdot a_p^2 \quad (3)$$

Figure 3 describes the dependence of the Vickers hardness of the substrate and the coating on the feed per tooth, according to the approximation relations (4) and (5).

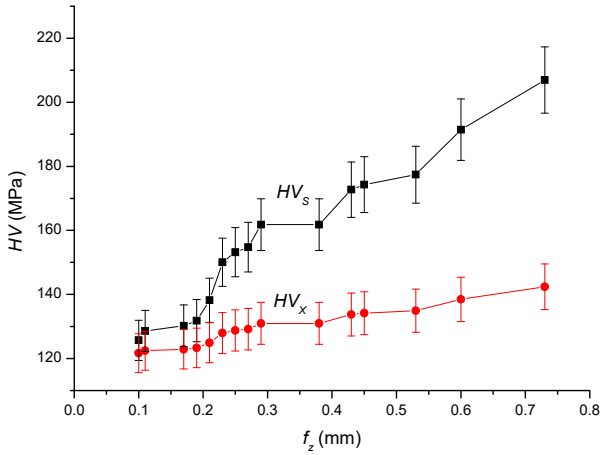

Figure 3. Dependence of Vickers hardness on the feed per tooth (HV_S—substrate Vickers hardness; HV_X—spray Vickers hardness).

Equation (4) applies to substrate Vickers hardness and Equation (5) applies to spray Vickers hardness at the feed per tooth with an accuracy of $R^2 = 0.96$:

$$HV_S = 108.76 + 170.18 \cdot f_z - 14.39 \cdot f_z^2 \quad (4)$$

$$HV_X = 117.33 + 43.95 \cdot f_z - 14.39 \cdot f_z^2 \quad (5)$$

Figure 4 describes the dependence of substrate Vickers hardness and the coating on the speed of cut, according to the approximation relations (6) and (7).

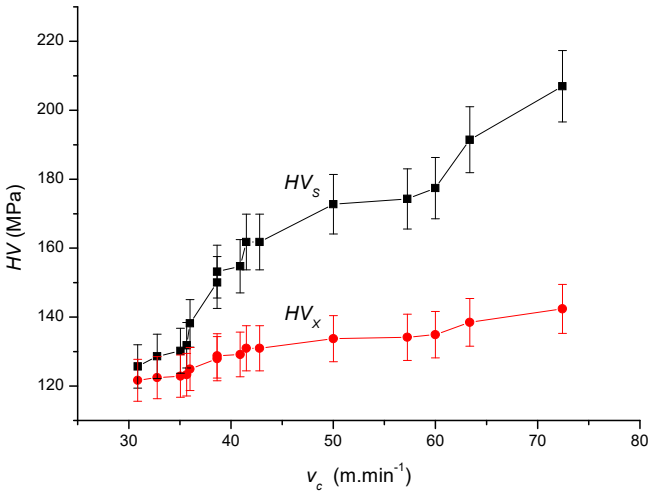

Figure 4. Dependence of the Vickers hardness on cutting speed (HV_S—substrate Vickers hardness; HV_X—spray Vickers hardness).

Equation (6) applies for substrate Vickers hardness and Equation (7) applies to spray Vickers hardness on cutting speed with an accuracy of $R^2 = 0.94$:

$$HV_S = 18.15 + 4.23 \cdot v_c - 0.024 \cdot v_c^2 \quad (6)$$

$$HV_X = 93.91 + 1.09 \cdot v_c - 0.01 \cdot v_c^2 \quad (7)$$

3. Results and Discussion

3.1. Ratio of Machining Parameter

In the context of the relative parameter ratio of the machining parameter R_{mp} (8), the following parameters were newly introduced: the ratio of the surface roughness machining parameter R_{mpR_a} (9), predicted surface roughness R_{a_P} (10), the ratio of the machining parameter to adhesion stress $R_{mpA_{dh}}$ (11), and finally adhesion stress A_{dh} (13). It is an integrated evaluation of the complex influence of cutting parameters on the mechanical state in the cut and, at the same time, also on the topographic state of the final surface after cutting.

$$R_{mp} = \left(\frac{f_z}{f_{z0}} \cdot \frac{v_c}{v_{c0}} \cdot \frac{a_p}{a_{p0}} \right) \quad (8)$$

$$R_{mpR_a} = \left(\frac{f_z}{f_{z0}} \cdot \frac{v_c}{v_{c0}} \cdot \frac{a_p}{a_{p0}} \cdot \frac{R_a}{R_{a_0}} \right) \Rightarrow R_{mpR_a} = \frac{R_{mp}}{R_{mp0}} \cdot \frac{R_a}{R_{a_0}} \quad (9)$$

$$R_{a_P} = R_{a_0} \cdot \frac{R_{mpR_a}}{\left(\frac{f_z}{f_{z0}} \cdot \frac{v_c}{v_{c0}} \cdot \frac{a_p}{a_{p0}} \right)} \Rightarrow R_{a_P} = R_{a_0} \cdot \frac{R_{mpR_a}}{R_{mp}} \quad (10)$$

$$R_{mpA_{dh}} = \left(\frac{f_z}{f_{z0}} \cdot \frac{v_c}{v_{c0}} \cdot \frac{a_p}{a_{p0}} \cdot \frac{A_{dh}}{A_{dh0}} \right) \Rightarrow R_{mpA_{dh}} = \frac{R_{mp}}{R_{mp0}} \cdot \frac{A_{dh}}{A_{dh0}} \quad (11)$$

In the case of R_{mpR_a}, it is the ratio of the currently selected cutting parameters and the parameters calculated or graphically constructed for the neutral plane at a depth of cut on the neutral plane a_{p0}. The parameters feed per tooth on the neutral plane f_{z0}, speed of cut on the neutral plane v_{c0}, the depth of cut on the neutral plane a_{p0}, surface roughness on the neutral plane R_{a0}, and others are material parameters, i.e., R_{mpR_a} and $R_{ampA_{dh}}$. These are ratios of currently selected values and values of given material parameters. Therefore, the derived parameters R_{mpR_a} and $R_{ampA_{dh}}$ can accurately express the instantaneous state of the mechanical tool−material interaction in the contact area, according to (9), (11). In principle, it is physically the ratio of the material cut to the volume of the theoretical material removal, precisely at the neutral depth of cut on the neutral plane a_{p0}. The values of the ratio of the machining parameter on the neutral plane R_{mp0} (in the area where the values of tensile and compressive stress are equal) must be calculated specifically for each material in conjunction with the neutral values v_{c0}, f_{z0}, a_{p0}. However, the surface roughness on the neutral plane is the same for all materials: $R_{a0} = 3.70$ µm. In the presented measurements, the following applies to the neutral plane of steel EN 10060: $v_{c0} = 103.31$ m·min^{-1}, $f_{z0} = 0.74$ mm, $a_{p0} = 0.22$ mm.

The newly introduced parameters R_{mp} and R_{a_P} integrate the complex influence of the set of selected cutting parameters on the mechanical state in the cut and, at the same time, also on the topographic state of the final surface after the cut. In the case of the parameter R_{mpX} (product of selected cutting parameters), it is the ratio of the currently selected cutting parameters and the parameters calculated or graphically constructed for the neutral plane R_{mp0} at a depth of cut on the neutral plane a_{p0} (12).

$$R_{mp} = \frac{R_{mpX}}{R_{mp0}} \quad (12)$$

The relative machining parameter related to the neutral plane, i.e., in the area where the values of tensile and compressive stress are equal, is $R_{mp0} = 1$.

3.2. Adhesive Stress

For the newly presented relation (13) of a simple, discrete evaluation of the adhesive stress A_{dh} (based on the input technological parameters), an adequate relation (14) (based on the surface morphology) applies [19]. This relation is based on simple mechanics, where it is a suitable/adequate ratio between the surface roughness of the machined substrate R_a (μm) and the structural grain size D_{gr} (μm) of the coating.

$$A_{dh} = A_{dh_0} \cdot \frac{R_{mpA_{dh}}}{\left(\frac{f_z}{f_{z0}} \cdot \frac{v_c}{v_{c0}} \cdot \frac{a_p}{a_{p0}}\right)} \Rightarrow A_{dh} = A_{dh_0} \cdot \frac{R_{mpA_{dh}}}{R_{mp}} \tag{13}$$

$$A_{dh} = 10^{-2} \cdot \frac{R_a}{D_{gr}} \cdot \sqrt{E_{mSUB} \cdot E_{mCOV}} \cdot k_{por} \tag{14}$$

The values of the parameters in the relation (14) can be determined relatively simply and discretely:

A_{dh} adhesive stress, i.e., the adhesive stress acting on the grain area of the coating [MPa],
D_{gr} size/diameter of the structural grain of the coating [μm],
E_{mSUB} Young's modulus of elasticity of the substrate material [MPa],
E_{mCOV} Young's modulus of elasticity of the coating material [MPa],
k_{por} degree of porosity of the coating according to the spraying technique [–].

By evaluating the relation (14), it is possible to express the adhesion on the neutral plane h_0, or in the depth of cut on the neutral plane a_{p0}, i.e., to express the user-desired adhesion between the substrate used (steel EN 100 60) and the coating used (nickel alloy NiCrBSi), at the value $k_{por} = 1$ (15):

$$A_{dh0} = 10^{-2} \cdot \frac{R_a}{24.65} \cdot \sqrt{347,050 \times 206,000} \times 1 = 401.4 \tag{15}$$

Therefore, adhesive stress A_{dh0} on the neutral plane h_0, or in the depth of cut on the neutral plane a_{p0}, has a specific value of 401.4 MPa. The dependence of the adhesive stress A_{dhX} on the depth of cut is described in Figure 5, according to the approximation relation (16), with excellent accuracy of measurement (0.93).

$$A_{dhX} = -347.80 + 1397.81 \cdot a_p - 427.63 \cdot a_p^2 \tag{16}$$

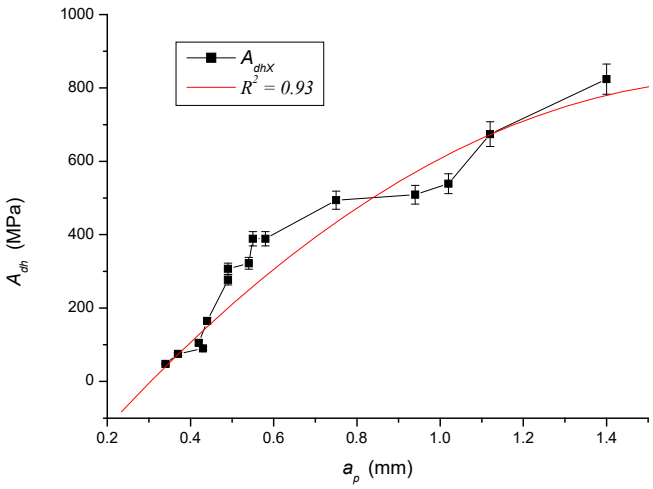

Figure 5. Dependence of adhesive stress on the depth of cut.

Now the solution can be assumed as follows:

(a) Utilizing other advantages of the newly derived parameter R_{mp} ($mm^3 \cdot min^{-1}$), it is possible to evaluate analogically and illustrate direct connections to specific cutting parameters, or to other parameters according to the presented implicit expression $A_{dh} = f \cdot (f_z, v_c, a_p \ldots)$.

(b) Based on the above findings, the "adhesive potential of the substrate" can also be newly designed for the needs of applied research (17):

$$A_{dhS_0} = \left(10^{-2} \cdot R_{a_0} \cdot \sqrt{E_{mSUB}} \cdot k_{por}\right)^2 \quad (17)$$

Based on such an accurately evaluated adhesion potential of the substrate, the most suitable coating material can be precisely selected from the point of view of the need to obtain solid adhesion. The adhesive potential of the substrate A_{dhS0} on the neutral plane h_0, or in the depth of cut on the neutral plane a_{p0} after substituting the values of the subject parameters (k_{por} = 1, E_{mSUB} = 347,050 MPa) into the relation (17) is 476.1 MPa. In conclusion, it can be stated that the specific value of the adhesive potential of the investigated substrate has a comparative information value from the point of view of industrial needs.

3.3. Comparison and Verification of Adhesion Measurement Results

The calculated values of the adhesiveness A_{dh} and the corresponding measured surface roughness R_a was given in relation to the measured depths of cut a_p. In particular, it can be seen from Figure 6 that with the depth of cut, the surface adhesion increases relatively steeply, while the surface roughness of the coating is approximately constant. What plays an important role for the adhesion of the coating surface in the cut depth of a given depth is not only the roughness of the coating but also the roughness of the substrate, especially in the region of the depth of cut approaching the thickness of the coating. The adhesion of the coating surface has a specific comparative information value about the adhesion forces as attractive intermolecular chemical and physical forces in the irregularities and pores of the coating surface of the investigated material.

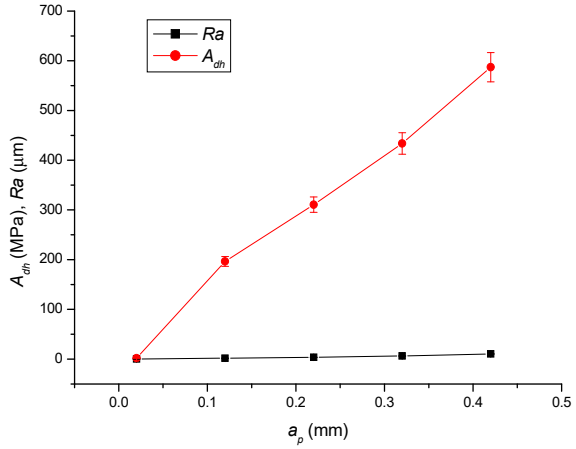

Figure 6. Dependence of adhesiveness and surface roughness on the depth of cut.

3.4. Vickers Hardness

In connection with the measurement of Vickers hardness, reference can be made to the derivation of the approximation for the dependence of the Vickers hardness on Young's modulus of elasticity $HV = f \cdot (E_{mat})$. The obtained approximation (Figure 7) is derived according to the Mohs hardness scale leading to the relation (18):

$$HV = 1201.33 + 8.82 \cdot 10^{-5} \cdot E_{mat} + 8.77 \cdot 10^{-9} \cdot E_{mat}^2 \quad (18)$$

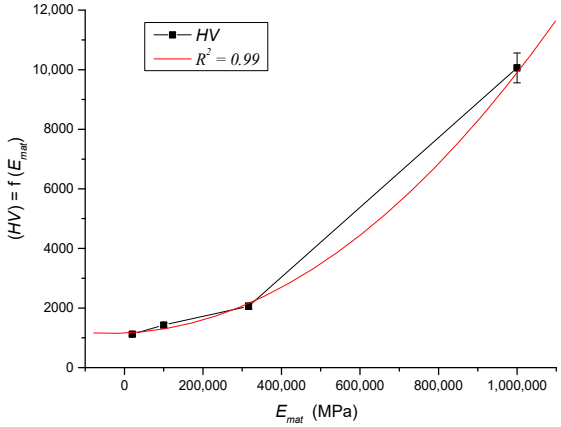

Figure 7. Control comparison of values $(HV) = f \cdot (E_{\mathrm{mat}})$.

3.5. Comparison and Verification of Vickers Hardness Measurement Results

Comparisons and verifications of *HV* Vickers hardness values were performed. Table 4 shows the numerical comparison and verification of the obtained data and Figure 8 shows their adequate graphical comparison, where the individual parameters are: HV_{sub} substrate Vickers hardness, HV_{T} theoretically calculated Vickers hardness according to Equation (18), and HV_{M} measured Vickers hardness.

Table 4. Numerical comparison and verification of Vickers hardness.

a_{p} mm	HV_{sub} MPa	HV_{T1} MPa	HV_{T2} MPa	HV_{M1} MPa	HV_{M2} MPa
0.01	179	437	455	200	210
0.10	179	475	476	375	400
0.20	179	648	1891	680	1860
0.30	179	743	496	780	500
0.40	179	765	491	800	480
0.50	179	722	1386	760	1580
0.60	179	770	934	805	1230
0.70	179	665	731	700	1000
0.80	179	593	606	610	800
0.90	179	743	3066	780	2330
1.00	179	754	1418	790	1600
1.10	179	765	2779	800	2230
1.20	179	527	1111	500	1385
1.30	179	601	1295	620	1520
MEDIAN	**179**	**658**	**1224**	**657**	**1223**

(HV_{T1}, HV_{M1} for the NiCrBSi coating; HV_{T2}, HV_{M2} for the NiCrBSi–WC coating).

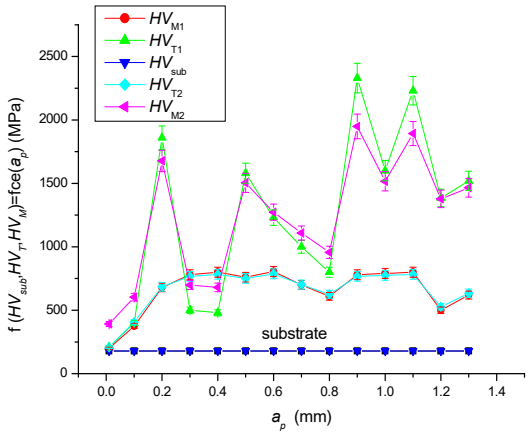

Figure 8. Demonstration of Vickers hardness changes along with the depth of cut of the steel substrate and NiCrBSi/NiCrBSi–WC coatings.

3.6. Tensile Stress

Based on the relation (1), own measurement results, analyses and interpretations of obtained measurement results, a parameter characterizing tensile stress σ_{rz} can be introduced, which can be expressed by the relation (19) after modifications [27,28].

$$\sigma_{rz} = 10^{-3} \cdot E_{mat} \cdot \frac{R_a}{R_{a_0}} = 10^{-3} \cdot \frac{F}{d^2} = \frac{HV}{0.189} \tag{19}$$

The parameter σ_{rz} can be expressed using the above parameter R_{mp}, which is related to the technological parameters of milling, according to the relation (20):

$$\sigma_{rz} = \sigma_{rz0} \cdot \frac{R_{mp_{\sigma rz}}}{R_{mp}} \tag{20}$$

where the relation (21) applies:

$$R_{mp_{\sigma rz}} = R_{mp} \cdot \frac{\sigma_{rz}}{\sigma_{rz0}} \tag{21}$$

3.7. Comparison and Verification of Tensile Stress Measurement Results

Figure 9 presents a comparison of stress changes along with the depth of cut a_p of a steel substrate, NiCrBSi and NiCrBSi–WC coatings.

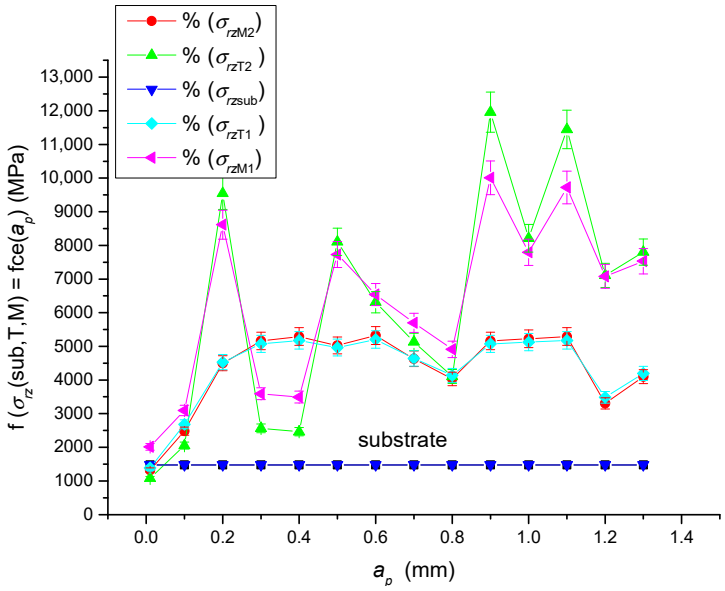

Figure 9. Comparison of stress changes along with the depth of cut a_p.

4. Interpretation of Data Using Adhesiveness and Relative Machining Parameter

Based on the measured data and their analysis, new prediction Equations (8)–(13) and (17) were created. Table 5 illustratively shows the calculated values of R_{ap} roughness, A_{dh} adhesion stress and R_{mpX} relative machining parameter, in the context of the measured R_{asub} values

Based on the subject data analysis, classification into individual sections of adhesiveness was possible, based on the relative machining parameter R_{mp} (Figure 10):

- section A (E_{xpNO} 1–6) insufficient surface roughness for the required adhesion,
- section B (E_{xpNO} 7–9) suitable surface roughness for the required adhesion,
- section C (E_{xpNO} 10–15) excellent surface roughness for the required adhesion.

Table 5. Numerical comparison and verification of Vickers hardness.

E_{xpNo}	R_{asub} µm	R_{ap} µm	A_{dh} MPa	R_{mpX} mm^3·min^{-1}
1	3.56	2.99	165	15.80
2	1.94	1.63	90	10.10
3	2.27	1.90	105	11.30
4	1.62	1.36	75	9.00
5	5.99	5.03	277	20.00
6	1.04	0.87	48	5.00
7	11.01	9.25	509	31.30
8	17.81	14.96	824	45.00
9	6.96	5.85	322	25.00
10	8.42	7.07	389	30.00
11	6.64	5.58	307	25.00
12	8.42	7.07	389	37.50
13	11.66	9.79	539	30.00
14	14.57	12.24	674	37.50
15	10.69	8.98	494	31.30

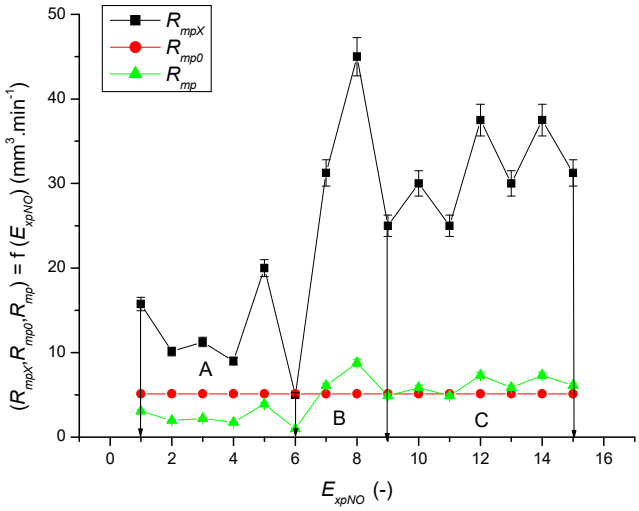

Figure 10. Graph of selected values of R_{mp}, R_{mp0} and R_{mpX} as the function (E_{xpNo}) for NiCrBSI alloy.

As an example of the calculation of surface roughness $R_a = f{\cdot}(E_{xpNO})$ for EN 10060 substrate and spraying material NiCrBSi alloy to use the parameter R_{mp}, a graph of the distribution of discrete values R_a according to Figure 11 can be presented, which depends on the direct relation to individual cutting parameters according to Table 3, see also Table 5. The calculation of the values of the graph in Figure 11 was performed according to the above-declared relations (9) and (10).

The surface roughness parameter R_a is a significant parameter for us and is also frequently used in our application calculations and in our newly derived relations. The importance of R_a roughness for application calculations is elaborated in great detail in our patent specifications [29,30]. This article deals, for example, with the calculation of adhesion A_{dh} (14), with the applied calculation of roughness $R_{ap} = f\ (R_{mp}, v_c, f_z, a_p)$ (10), as well as with the calculation of surface stresses $\sigma_{rz} = f\ (R_a, R_{a0}, E_{mat})$ (19). Equation (19) declares a new relation to the Vickers hardness $HV = f\ (R_a, \sigma_{rz})$, which has been compared and verified with the literature [29,30], as presented in Section 3.

The new relations mentioned above describing the relationships between technological, textural, stress-strain parameters and optimal parameters characterizing the milling technology (a_p, f_z, v_c) are based on the newly introduced parameter R_{mp}, which is applied in various modifications, namely in relations (8) to (11), (13) and (21). Using this relative technological parameter R_{mp}, it was also possible to reclassify the adhesive sections (Figure 10).

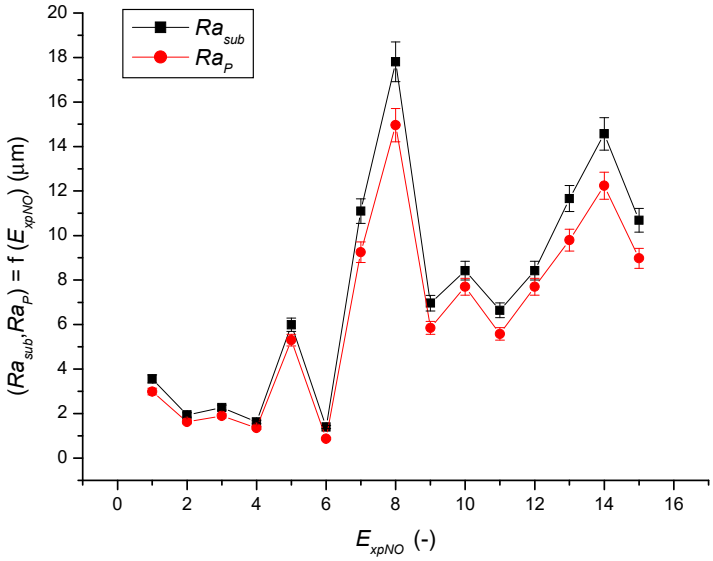

Figure 11. Roughness R_a of EN 100 60 substrate and spraying NiCrBSi alloy according to R_{mp} for E_{xpNO}.

5. Summary

The aim of the presented publication was to predict and classify the technological parameters of milling a spherical substrate of steel EN 10060 after HVOF spraying of NiCrBSi nickel alloy, especially in connection with the prediction of adhesive stress between the substrate and the coating.

1. Based on the analysis and interpretation of measured data, the newly created predictive relationships were specified:
   - the relative technological parameter ratio—machining parameter R_{mp},
   - the ratio of the surface roughness machining parameter R_{mpR_a},
   - the predicted surface roughness R_{aP},
   - the ratio of the machining parameter to adhesion stress $R_{mpA_{dh}}$,
   - the adhesion stress A_{dh},
   - the ratio of the currently selected cutting parameters and the parameters calculated or graphically constructed for the neutral plane R_{mp0} at a depth of cut on the neutral plane a_{p0},
   - the adhesive potential of the substrate A_{dhS0}.
2. In particular, the traditional roughness parameters and newly predicted relative machining parameters and adhesive stress parameters were the basis for classification into three basic "adhesion sections".
3. Selected cutting parameters (the speed of cut v_c, the feed per tooth f_z, the depth of cut a_p) can be considered basic from a technology point of view because they directly determine the volume of material removed, the texture of the machined surface, as well as the instantaneous stress state between the substrate and the coating when the tool comes into contact with the disintegrated material, i.e., they determine the degree of adhesion of the substrate and machined coating.
4. Evaluated distribution functions of selected cutting parameters (v_c, v_{c0}, f_z, f_{z0}, a_p, a_{p0}) for calculating relative technological parameters of machining (R_{mp}, R_{mp0}) and consequently parameters of adhesive stress (A_{dh}, A_{dh0}) allow plotting courses of distribution functions in connection with the depth of cut a_p and also in connection with other parameters essential from a technology point of view. In principle, it is an elaborate analytical description of the stress state at the tool–material contact, i.e., a specifically linked complex of functions describing the mechanism of the machining process.

The main presented results are new relationships describing the relation between individual technological, textural, and stress-strain parameters, classification of adhesive sections and determination of optimal milling conditions based on the identification of adhesive sections using derived equations.

Author Contributions: Conceptualization, J.V. and M.H.; methodology, M.K. and J.Ř.; validation, J.F. (Jaroslava Fulemová) and M.G.; formal analysis, M.H.; investigation, L.K. and J.H.; data curation, J.F. (Jan Filipenský); writing—original draft preparation, J.V.; writing—review and editing, M.H. and M.K.; funding acquisition, J.Ř. All authors have read and agreed to the published version of the manuscript.

Funding: The present contribution has been prepared under project ED2.1.00/19.0391 'Development of machining technologies in RTI' under the auspices of the Research and Development for Innovation of the Ministry of Education, Youth and Sports of the Czech Republic aimed to support research, experimental development and innovation.

Conflicts of Interest: The authors declare no conflict of interest.

References

1. Buytoz, S.; Ulutan, M.; Islak, S.; Kurt, B.; Çelik, O.N. Microstructural and wear characteristics of high velocity oxygen fuel (HVOF) sprayed NiCrBSi–SiC composite coating on SAE 1030 steel. *Arab. J. Sci. Eng.* **2013**, *38*, 1481–1491. [CrossRef]
2. Islak, S.; Buytoz, S.; Kurt, B. Microstructural characteristics of high velocity oxygen fuel (HVOF) sprayed NiCrBSi–SiC composite coating on a low alloy steel. In Proceedings of the 6th International Advanced Technologies Symposium (IATS'11), Elazığ, Turkey, 16–18 May 2011.
3. Afsous, M.; Shafyei, A.; Soltani, M.; Eskandari, A. Characterization and Evaluation of Tribological properties of NiCrBSi–Gr composite coatings deposited on stainless steel 420 by HVOF. *J. Therm. Spray Technol.* **2020**, *29*, 773–788. [CrossRef]
4. Stewart, S.; Ahmed, R.; Itsukaichi, T. Rolling contact fatigue of post-treated WC–NiCrBSi thermal spray coatings. *Surf. Coat. Technol.* **2005**, *190*, 171–189. [CrossRef]
5. Pawlowski, L. *The Science and Engineering of Thermal Spray Coatings*, 2nd ed.; John Wiley & Sons: Hoboken, NJ, USA, 2008.
6. Lisiecki, A. Tribology and surface engineering. *Coatings* **2019**, *9*, 663. [CrossRef]
7. Planche, M.P.; Liao, H.; Normand, B.; Coddet, C. Relationships between NiCrBSi particle characteristics and corresponding coating properties using different thermal spraying processes. *Surf. Coat. Technol.* **2005**, *200*, 2465–2473. [CrossRef]
8. Modi, S.C.; Calla, E. Structure and properties of HVOF sprayed NiCrBSi coatings. In *Thermal Spray 2001: New Surfaces for a New Millennium, Singapore, 28–30 May 2001*; Berndt, C.C., Khor, K.A., Lugscheider, E., Eds.; ASM International: Materials Park, OH, USA, 2001.
9. Garrido, M.A.; Rico, A.; Gómez, M.T.; Cadenas, M.; Fernández-Rico, J.E.; Rodríguez, J. Tribological and oxidative behavior of thermally sprayed NiCrBSi coatings. *J. Therm. Spray Technol.* **2017**, *26*, 517–529. [CrossRef]
10. Niranatlumpong, P.; Koiprasert, H. Phase transformation of NiCrBSi–WC and NiBSi–WC arc sprayed coatings. *Surf. Coat. Technol.* **2011**, *206*, 440–445. [CrossRef]
11. Zouari, S.; Ghorbel, H.; Danlos, Y.; Liao, H.; Elleuch, R. Comparative study of HVOF-Sprayed NiCrBSi alloy and 316L stainless steel coatings on a brass substrate. *J. Therm. Spray Technol.* **2019**, *28*, 1284–1294. [CrossRef]
12. Miguel, J.M.; Guilemany, J.M.; Vizcaino, S. Tribological study of NiCrBSi coating obtained by different processes. *Tribol. Int.* **2003**, *36*, 181–187. [CrossRef]
13. Gonzalez, R.; Cadenas, M.; Fernandez, R.; Cortizo, J.L.; Rodríguez, E. Wear behaviour of flame sprayed NiCrBSi coating remelted by flame or by laser. *Wear* **2007**, *262*, 301–307. [CrossRef]
14. Houdková, Š.; Smazalová, E.; Vostřák, M.; Schubert, J. Properties of NiCrBSi coating, as sprayed and remelted by different technologies. *Surf. Coat. Technol.* **2014**, *253*, 14–26. [CrossRef]
15. Chaliampalias, D.; Vourlias, G.; Skolianos, S.; Polychroniadis, E.K.; Stergioudis, F. Surface microstructure of NiCrBSi coatings deposited by flame spray and evaluation of the oxidation resistance. *Solid State Phenom.* **2010**, *163*, 51–54. [CrossRef]

16. Usana-ampaipong, T.; Dumkum, C.; Tuchinda, K.; Tangwarodomnukun, V.; Teeraprawatekul, B.; Qi, H. Surface and subsurface characteristics of NiCrBSi coating with different WC Amount prepared by flame spray method. *J. Therm. Spray Technol.* **2019**, *28*, 580–590. [CrossRef]
17. Roy, M.; Davim, J.P. *Thermal Sprayed Coatings and their Tribological Performances*, 1st ed.; IGI Global: Hershey, PA, USA, 2015.
18. Zhang, Y.; Li, W.; Zhang, C.; Liao, H.; Zhang, Y.; Deng, S. A spherical surface coating thickness model for a robotized thermal spray system. *Robot. Comput.-Integr. Manuf.* **2019**, *59*, 297–304. [CrossRef]
19. Chen, Z.; Etsion, I. Recent development in modeling of coated spherical contact. *Materials* **2020**, *13*, 460. [CrossRef]
20. Chen, L.; Liang, Y.-Y.; Luo, J.-B.; Zhang, C.-H.; Yang, G.G. Mathematical modeling and experimental study on photoresist whirl-coating in convex-surface laser lithography. *J. Opt. A Pure Appl. Opt.* **2009**, *11*, 105408. [CrossRef]
21. Feng, X.G.; Sun, L.C. Mathematical model of spin-coated photoresist on a spherical substrate. *Opt. Express* **2005**, *13*, 7070–7075. [CrossRef]
22. Liu, H.; Fang, X.; Meng, L.; Wang, S. Spin coating on spherical surface with large central angles. *Coatings* **2017**, *7*, 124. [CrossRef]
23. Lin, M.C.; Chang, L.S.; Lin, H.C.; Yang, C.H.; Lin, K.M. A study of high-speed slurry erosion of NiCrBSi thermal-sprayed coating. *Surf. Coat. Technol.* **2006**, *201*, 3193–3198. [CrossRef]
24. Karimi, M.R.; Salimijazi, H.R.; Golozar, M.A. Effects of remelting processes on porosity of NiCrBSi flame sprayed coatings. *Surf. Eng.* **2016**, *32*, 238–243. [CrossRef]
25. Rachidi, R.; El Kihel, B.; Delaunois, F. Microstructure and mechanical characterization of NiCrBSi alloy and NiCrBSi–WC composite coatings produced by flame spraying. *Mater. Sci. Eng. B* **2019**, *241*, 13–21. [CrossRef]
26. Rachidi, R.; El Kihel, B.; Delaunois, F.; Vitry, V.; Deschuyteneer, D. Wear performance of thermally sprayed NiCrBSi and NiCrBSi–WC coatings under two different wear modes. *J. Mater. Environ. Sci.* **2017**, *8*, 4550–4559. [CrossRef]
27. Valíček, J.; Harničárová, M.; Řehoř, J.; Kušnerová, M.; Gombár, M.; Drbúl, M.; Šajgalík, M.; Filipenský, J.; Fulemová, J.; Vagaská, A. Prediction of cutting parameters of HVOF-Sprayed Stellite 6. *Appl. Sci.* **2020**, *10*, 2524. [CrossRef]
28. Valíček, J.; Řehoř, J.; Harničárová, M.; Gombár, M.; Kušnerová, M.; Fulemová, J.; Vagaská, A. Investigation of surface roughness and predictive modelling of machining Stellite 6. *Materials* **2019**, *12*, 2551. [CrossRef] [PubMed]
29. Valíček, J.; Borovička, A.; Hloch, S.; Hlaváček, P. Method for the Design of a Technology for the Abrasive Waterjet Cutting of Materials. U.S. Patent 9,073,175, 7 July 2015.
30. Valíček, J.; Borovička, A.; Hloch, S.; Hlaváček, P. Method for the Design of a Technology for the Abrasive Waterjet Cutting of Materials Kawj. Czech Republic Patent CZ 305514 B6, 23 July 2010.